Click to View Poster

Onshore Structural Movement Revealed Through the Presence of Volcaniclastic Deposition Offshore. Cholula-1EXP, Miocene Salina del Istmo Basin, Mexico.

David 'Stan' Stanbrook[1], Nicola Capuzzo[2], Michael Durcanin[1], Brian LeCompte[1], Gabriel Perez[1], Craig Farley[1], and Adam Seitchik[1]

Search and Discovery Article #51692 (2022)**
Posted August 4, 2022

*Adapted from extended abstract based on oral presentation given at 2019 AAPG Annual Convention and Exhibition online meeting.
 DOI:10.1306/51692Stanbrook2022

[1]Murphy Exploration & Production Company, Houston, USA
[2]Task Fronterra Geoscience, Houston, Texas

Introduction

In February of 2019 Murphy Sur drilled the Cholula-1EXP wildcat discovery-well in Block 5 within the Salina del Istmo Basin, southern Gulf of Mexico (Figure 1). The well was positioned slightly off the crest of a complex compressional salt-structure and encountered 64m net pay in a Late Miocene turbidite sandstone succession. The well drilled to a total depth of 2746m penetrating Late, Middle and Early Miocene strata.

Post-well analysis of wireline logs, cuttings, and sidewall cores indicated multiple episodes of volcaniclastic deposition from the Burdigalian through to the Messinian, with the majority of volcaniclastics found within the lower parts of the Langhian, mid & upper Serravallian. Only one episode of volcaniclastic material was noted within the Tortonian interval though it seems likely that their recognition has been obscured by significant amounts of sand deposited by turbidity currents.

Standard petrophysical analysis revealed the presence of multiple layers of volcaniclastic material within the Miocene, having a typical low density & high resistivity expression. Image-log also detected the volcanics through a similar resistivity response but at a higher resolution. The identification of the log-derived volcaniclastics was confirmed though rotary side-wall core analysis and thin-section examination. The appearance of the volcaniclastic material in thin-section is of well-preserved acicular volcanic glass implying relatively little transport or reworking. We interpret these to have been derived from volcanic ash-fall that settled though the water-column to be buried on the seafloor. We also identify a single pulse of volcaniclastic in the Tortonian in which the acicular fragments appear more broken and mixed with other sediment. We believe that this material has undergone some form of physical transport either in turbidity currents or possibly through the action of geostrophic currents.

The occurrence of these episodes of volcaniclastics deposition coincides with or closely post-dates important stratigraphic boundaries. The cluster of volcaniclastics in the lower Langhian occurs after a sequence boundary marking the base of that stage. More importantly is a cluster of volcaniclastics that occur after a significant unconformity and hiatus in the Middle Miocene at the Langhian-Serravallian boundary. The most abundant interval of volcaniclastics terminates at the base of the Tortonian, coinciding with a change in bathymetry as recorded through biostratigraphy.

We believe that the volcaniclastics seen in the Cholula-1EXP well is a result of compression onshore at the onset of the Chiapanecan Orogeny, resulting from the subduction of the Cocos Plate beneath the North American plate (Gutiérrez-Paredes et al, 2018) and the volcanic activity that resulted from this subduction event. Further we believe that the presence of volcaniclastics that tie to sequence boundaries in the offshore present opportunities to enhance regional correlations in the Salina del Istmo Basin.

Regional Geologic Setting

Block 5 lies within the Salina del Istmo Basin, southern Gulf of Mexico (Figure 1). The tectonic evolution the Salina del Istmo Basin relates to regional tectonic events during the evolution of the Gulf of Mexico (Figure 2). Overall the tectonic history of the southern Gulf of Mexico is strikingly different from its northern counterpart. Gutierrez Paredes et. al (2017) provide a thorough summary of the regional tectonic history starting with subduction of the Farallon Plate under the North American Plate during the Laramide Orogeny, the subsequent movement of the Chortis Block, and the final subduction of the Cocos Plate under the southern end of North America leading to the formation of the passive continental margin from the Late Miocene until today.

Paleogene clastic sedimentation in the southern Gulf of Mexico derived from the Chiapas Massif which produced large volumes of sediment into this deep-water setting while contemporaneously deposition of shallow water carbonates continued in the Yucatan Block (Padilla y Sánchez, 2007). Angeles-Aquino et al (1994) suggest that salt movement combined with the lowering of sea level produced a regional unconformity in the middle and late Oligocene. The Miocene succession is characterized by gravity-driven depositional processes including turbidite and mass-transport deposits as well hemipelagic sediments that fill local sub-basins formed by deformation of Callovian salt sequences. Compression, related to the onset of the Chiapaneacan Orogeny in the Middle Miocene, created widespread folding and faulting of Early Miocene and older strata (Sanchez-Montes de Oca, 1980). The shortening was a result of lateral movement of the Chortis Block and the subduction of the Cocos Plate beneath the North American Plate. Later these structures were tilted to the north-northwest when the Callovian salt was mobilized northward resulting in new depocenters and minibasins.

The migration of the Chortis Block along the Pacific Margin of Mexico was accompanied by the displacement of volcanism. Active volcanic centres during the deposition of Miocene volcanics observed in Cholula-1EXP include the Sierra Madre del Sur, the Trans Mexican Volcanic Belt, the Eastern Alkaline Province and, as a far-field option, the Sierra Madre Occidental. This period also coincides with the onset of the Chiapanecan Orogeny, Chiapanecan Deformation and Salina del Istmo salt tectonics (Figure 3).

Sub-aqueous volcaniclastic processes and terminology

Volcaniclastic particles result from fragmentation of volcanic material both during and after volcanic activity though transportation processes (Figure 4). Summarised primary volcaniclastic particles (Burley et al, in prep) include:

a. Pyroclasts –form by explosive fragmentation of the magma into particles (including ash, highly vesiculated glass (pumice/scoria), crystals
   and crystal fragments, and lithic fragments)
b. Hydroclasts–form by explosive interaction with external water (via phreatic and phreato-magmatic explosions) or by non-explosive quenching and granulation of lava (lava flows and shallow subsurface intrusions)
c. Autoclasts–form by frictional breakage of moving viscous lava flows

Cholula-1EXP Description

Geological setting

Murphy Sur & partners drilled the Cholula-1EXP wildcat discovery-well in Block 5 within the Salina del Istmo Basin, southern Gulf of Mexico in February of 2019 (Figure 1). The well is located in the southeastern corner of the block and lies 35.5km due north from the nearest well to the south, Zama-1, a major Upper Miocene hydrocarbon discovery (Figure 1). Cholula-1EXP tested multiple reservoir targets in the Late, Middle and Early Miocene within a four-way dip closure. The formation of the Cholula structure initially formed due to Larimide shortening and continued to develop into the Early Pliocene. Mapping of growth strata over the crest of the Cholula structure suggest that shortening was episodic.

The well met its reservoir objectives by successfully encountering turbidite sandstones in the Miocene as well as establishing the location of the top Oligocene. The well successfully tested the presence of effective source rocks & migration pathways by encountering 64m of net oil and gas pay with hydrocarbons typed back to the predicted Mesozoic carbonates. The source rock is most likely Tithonian in age- see Farley et al, 2020 (this conference) for more information. Murphy Sur and its Block 5 partners plan to further test the Cholula-1EXP structure.

Stratigraphy & depositional environments

Post-drill biostratigraphic analysis confirmed the anticipated reservoir ages with adjustments to pre-drill stratigraphic tops typically less than 10m in true stratigraphic thickness (Figure 5). The analysis also confirmed the general depositional environment as deep-marine. Generally speaking, the Oligocene, Early Miocene & Middle Miocene were interpreted to be in an upper bathyal environment; it is with this period, during the Langhian and Serravallian, that the majority of volcaniclastics observed in Cholula-1EXP are found. Above this a significant Mid-Miocene unconformity from roughly 11.8 ma – 9.5 ma is observed. The Mid-Miocene unconformity also coincides with step-change decrease in palaeobathymetry from upper bathyal to outer neritic, the onset of a significant increase in clastic sediment flux as well as the termination of observed volcaniclastics until the mid-upper Tortonian.

Geophysical response

The amplitude of an event in a stack seismic image is governed to a large extent by the contrast in impedance across interfaces between rock units in the subsurface, where impedance is the product of density and velocity. Since the density of volcanic ash is anomalously low, ash deposits or other units with a relatively large content of ash might exhibit a relatively low seismic impedance, creating a large impedance contrast compared to surrounding rocks.
Because of their low impedance and if thick enough to be seismically visible, ash deposits or ash beds could then be associated to a bright amplitude event in a seismic profile. If judged solely on the bright character of the seismic amplitude, those might be hard to distinguish from other low-impedance events. Of interest for exploration, hydrocarbon sands are also in certain conditions expected to be low-impedance and bright seismic amplitudes ("bright spots") are commonly used as an indicator for the presence of hydrocarbons, or DHI for short.

The likelihood that seismic amplitude anomalies due to ash beds are attributed to the presence of hydrocarbons is then a risk factor for hydrocarbon exploration. The occurrence of such false positives has been reported elsewhere in the Gulf of Mexico (Friedman, 2006; Totten et al, 2005) and in our estimation is one of the possible explanations for the seismic amplitude anomalies targeted at the Lakmay-1 well in the Salina del Istmo basin. Matching our observations in the Cholula-1EXP well, compressional and shear wave velocities and their ratio are commonly considered not anomalous for ash beds. Those rock properties largely influence AVO response, so that AVO analysis and related techniques like simultaneous inversion, properly informed by local calibration, can be used to mitigate this risk.

We understand that closely spaced thick beds of volcaniclastics can produce a pronounced amplitude response as recorded in the examples above. In Cholula-1EXP however the amplitude response to the volcaniclastic is somewhat muted given that the beds are typically less than one metre thick and relatively widely spaced (Figure 6).

Petrophysical character of the Cholula-1EXP volcaniclastics

Petrophysical logs respond to the pore fluids and minerals that make up the subsurface. Logs are affected by borehole size, mud properties, bed thickness, and many other variables, many of which are accounted for in the environmental corrections of the logs. Once corrected, the logs represent an electrical signal that corresponds to a subsurface property. All log measurements are indirectly related to rock properties. In this paper we refer to Gamma Ray (GR), bulk density (RHOB), neutron porosity (NPHI), and deep resistivity (RD).

Logs measure the entire rock, pore and mineral. Yet in every type of subsurface formation, the minerals make up a greater percentage of the whole than the pore fluids. That is why most log values are sensitive to mineral composition more than porosity, especially density, acoustic, and neutron porosity. Resistivity and nuclear magnetic resonance (NMR) logs respond almost entirely to the pore fluid, though resistivity logs are much more affected by the type of measurement (induction vs. laterolog) and the direction of measurement. Given the sensitivity of various log measurements to both pore fluids and minerals, it is possible to make a matrix of log responses for pure minerals and fluids. An example of such a table is shown in Figure 7. The primary matrix minerals quartz, orthoclase, and albite are identified, while the clay minerals and porosity are lumped as "wet clay". The OBM filtrate and free water in the flushed (X) zone are measured by the shallow conductivity log and the shallow reading density and neutron logs. The unflushed (U) oil and water are measured by the deep conductivity log.

In the Salina del Istmo Basin, there are anomalous log responses that occur through the Miocene to the K-T boundary. They are characterized by very low density, high neutron porosity, and moderately high resistivity above the shale background (Figure 7c). Their thickness ranges from less than 1m to up to 10m for an individual event or bed. Often these have mineral fluorescence, but not hydrocarbon fluorescence despite the high resistivity. X-Ray Diffraction (XRD) analysis of sidewall cores taken in these intervals shows a mix of feldspar, quartz, and muscovite. Because XRD is only sensitive to crystalline material, the muscovite at times approaches 100%. This is inconsistent with a low bulk density of 1.6 – 1.8 g/cc because dry muscovite can have a grain density up to 2.8 g/cc. Instead an alternative explanation is needed. Analysis of the thin sections shows abundant volcanic glass present in the samples. This is invisible to the XRD since it is non-crystalline. The X-Ray Fluorescence (XRF) data show up to 68% SiO_2 in the samples with muscovite, despite muscovite having only 45 – 51% silicon dioxide. This is further proof of the presence of amorphous volcanic glass. Petrophysically, one needs to solve for a mineral that has low bulk density, high Si, high neutron porosity, and moderate resistivity response.

In Figure 7; table b, we see table a modified with a mineral for the volcanic ash present in the Salina del Istmo Basin has been added under the name “Special Mineral 2.” In a simpler model, the ash content could be flagged by setting a threshold of RHOB < 2 & NPHI > 0.5. This will effectively eliminate reservoir intervals since the apparent porosity is greater than what is physically possible. A sandstone with a bulk density of 2.0 would have an apparent porosity of 39%. It is important to include the ash bed or volcanic material in the mineral solver in order to avoid including it as potential pay. Without a mineral set aside for the ash beds, the ash beds will calculate out as very high porosity sandstones. Given their resistivity higher than background level, the result is several zones of potential pay. In cases where there is interbedded quartz, it may or may not be hydrocarbon charged.

Image log character

During the drilling of Cholula-1EXP high-resolution resistivity image log was acquired from 1740-2680m MD encompassing the entire Miocene section. Task Fronterra Geoscience (2019), retained to do independent interpretation of the image logs, also noted the presence of volcaniclastic materials. The volcaniclastics provided a very resistive static image response, reaching the limit of the dynamic range of the tool, and was associated with a characteristic density and porosity response as well as a high zeolite content in the CPI log (Figure 8). They occurred as relatively thin to thicker (up to ~0.9m thick) bedded and concordant layers enclosed mostly in mudstones. From image log analysis alone, it was not possible to determine whether the tuffs derived directly from volcanic ash fallout or if they represented volcaniclastic sediments redeposited by turbidity currents or derived from a mix of these two processes.

The Serravallian, which contains a significant proportion of the volcaniclastics found in Cholula-1EXP is very thick unit which is punctuated by several relatively thin and electrically resistive beds, up to circa 0.5m thick, which show a characteristic response in the neutron and density logs, and a high zeolite content in the CPI log. They are interpreted as volcanic-rich beds (tuffs), although their nature as volcanic ash fall layers or volcaniclastic sediments could not be determined. Their very conformable bedding with the surrounding mudrocks suggests possible fallout from volcanic ashes draping the seabed topography but their thickness, which reaches up to circa 0.5m, and frequency would favour a volcaniclastic nature. The distribution and thickness of all tuff layers identified in the succession below 2220m can be seen in Figure 6.

Within the Tortonian, towards the top of the image log study interval, is a thick succession of massive to poorly stratified and shallow dipping mudrocks associated with a period of background pelagic to hemipelagic sedimentation. The relatively resistive character of the borehole images in comparison to shales observed deeper in the succession, is likely related to a calcareous or marly nature of these mudrocks. Within this sequence is a single poorly stratified volcaniclastic bed, about 1m thick, that is bounded by thin argillaceous "sandstones" (Figure 9). The sandstone boundaries are concordant with nearby shale bedding, while slightly over steepened internal stratification in the volcaniclastic bed is likely associated with small-scale soft-sediment deformation (possibly dewatering). Initially, in the image log analysis this bed was interpreted as an isolated event of turbiditic sandstone deposition . However petrographic analysis of thin sections from rotary sidewall core highlighted the presence of volcanic glass shards.

For event 2 in the Tortonian the image-log did not initially identify the beds at 2020m as volcaniclastics. The image log did show a similar borehole response to the other volcaniclastics but didn't have the characteristic log or CPI response. Furthermore, they were associated with a small-scale fault which resulted in poor image quality and so they were initially classified as thin massive sandstones.

For event 1 in the Messinian the volcaniclastic bed was a more isolated and more resistive bed enclosed within thick mudrocks. It shows an overall poor image quality, limited resistivity contrast, and an usual thickness (~1m) in comparison to other volcaniclastic beds. RSWC 2 indicates that in fact this bed is a thick and isolated volcanic deposit likely associated to an exceptional explosive volcanic event.

XRD Analysis

To compliment the standard petrophysical analysis and image log analysis 34 rotary sidewall cores were acquired within the Miocene section. These cores were sent for various analysis including X-Ray Diffraction (XRD) and thin-section analysis, in part to help determine the mineralogy of the specimens. Three of the rotary sidewall cores were specifically targeted at beds that were thought to contain volcaniclastics, with one of the aims being to contribute to the evaluation of pay in the petrophysical workflow (see above).

The XRD work revealed anomalously high percentages of muscovite mica in samples numbers 2, 10, 30 & 31 (Figure 10). Muscovite is likely an altered product of original mineralogy and would later be reclassified as volcanic glass following the thin-section work. There is an appreciable difference in the volcanic mineralogy between samples from the Burdigalian-Serravallian (samples 30 & 31) and from the Tortonian (sample 10); notably in the percentage of 'muscovite'.

Rotary sidewall core 31

Rotary sidewall core sample thirty-one acquired at 2321m MD (Figure 11) was taken within a dense zone of thirteen volcaniclastic beds identified from image log analysis that constitute a total of 4.18m of volcaniclastic beds within a twenty-two-metre interval between 2312.30 and 2334.35 (middle Serravallian). While the accuracy of rotary sidewall core thirty one is subject to some uncertainty it's placement at 2321m means that it falls within an interval that is 77% volcaniclastic; while it is in theory possible that the rotary sidewall core was placed between volcanic beds it seems improbable that the core would contain no trace of volcaniclastic material.

The thin-section shows that the mineralogy the sample is composed of sheet-like very fine sand to coarse silt grained volcanic material (mainly volcanic glass and minor zeolites (Photos 1-4; Figure 11). Sporadic silt to fine sand-sized quartz, feldspars, glauconite and globigerinids are also observed. The sample also contains burrow-like structures filled by clay (Figure 11 Photos 1 and 2, from Al2 to 03) and exhibits less than 1% of isolated intra-fossilar porosity (Figure 11 Photos 1 and 2, H5). Diagenetically the sequence is interpreted as sedimentation of volcanic ash into a marine sedimentary environment, burial and partial alteration of volcanic glass and feldspars into clays. The thin section work classifies the sample as a tuffaceous shale.

We believe that the identification of rotary sidewall core sample 31 as volcaniclastics from petrophysics, image-log analysis, high mica-content in the XRD work means that the acicular nature of the grain texture seen in the thin-section indicate volcaniclastic origin. Given the preservation of the acicular character of the volcaniclastics we consider that the grains have not undergone significant transport distance. Further we conject that given the lack of transport signature that the grains here were either derived from a single turbidity current event with little or no staging in the hinterland or that they were deposited directly onto the sea-surface through ash-fall and are essentially ‘in-situ’.

Rotary sidewall core 30

Rotary sidewall core sample thirty acquired at 2267m MD (Figure 12) was taken within a zone of six volcaniclastic beds identified from image log analysis that constitute a total of 2.14m of volcaniclastic beds within a twenty-two-metre interval between 2266.73 and 2312.30m. These beds are within the upper Serravallian with the uppermost bed of the six being coincident with the Serravallian-Tortonian boundary. While the accuracy of rotary sidewall core thirty is subject to some uncertainty it’s placement at 2367m means that it falls within an interval that is 24% volcaniclastic; while it is in theory possible that the rotary sidewall core was placed outside of a volcanic beds it seems improbable that the core would contain no trace of volcaniclastic material.

The thin-section shows that the mineralogy of the sample is composed of sheet-like very fine sand to coarse silt grained volcanic material (mainly volcanic glass and minor zeolites (Photos 1-4; Figure 12). Sporadic silt to fine sand-sized quartz and feldspars are also observed (Figure 12; Photos 1 and 2; Photos 3 & 4, D10: plagioclase grain). The sample also contains sporadic glauconite grains (Figure 12; Photos 3 and 4, 05). The clay content is very low, occurring as rim cements coating glass and feldspar grains (Figure 12; Photos 3 and 4, D11). Sample has no visible porosity. Diagenetically the sequence is interpreted as sedimentation of volcanic ash into a marine sedimentary environment, burial and partial alteration of volcanic glass and feldspars into clays. The thin section work classifies the sample as a tuffaceous sandstone/siltstone.

We believe that the identification of rotary sidewall core sample 30 as volcaniclastics from petrophysics, image-log analysis, and high mica-content in the XRD work means that the acicular nature of the grain texture seen in the thin-section indicate volcaniclastic origin. Like sidewall core sample 30 we believe the preservation of the acicular character of the volcaniclastics means that the grains have not undergone significant transport distance. We also believe that the apparent lack of transport means the grains were either derived from a single turbidity current event with little or no staging in the hinterland or that they were deposited directly onto the sea-surface through ash-fall and are essentially also ‘in-situ’.

Rotary sidewall core 10

Rotary sidewall core sample thirty acquired at 2020m MD (Figure 13) was identified in standard petrophysical interpretation as volcaniclastic but not initially by the image log analysis (see above). The image log did show a similar borehole response to the other volcaniclastics but didn't have the characteristic log or CPI response and are associated with a fault which resulted in poor image quality and they were initially classified as thin massive sandstones. RSWC 10 indicates that in fact they are volcaniclastic beds. However, the rotary sidewall core identified the sample as potentially volcaniclastic due to the high 'muscovite' percentage identified in the XRD analysis (Figure 10). This bed lies within the mid-upper Tortonian.

The thin-section shows that the mineralogy of the sample is mainly composed by coarse silt to very fine sand-sized volcanic ash (Photos 1 to 4, Figure 13). The glass particles are characterized as being isotropic and angular shaped (Photos 3 and 4, Figure 13). Other minor minerals include detrital quartz, feldspars and disseminated pyrite. Skeletal components include planktonic foraminifera (globigerinids), that are well-preserved or fragmented. Remains of organic matter are locally observed within the matrix and the sample probably contain zeolites and clays as pore-filling material or replacing volcanic grains. Diagenetically the sequence is interpreted as the sedimentation of volcanic ash particles, burial, compaction and partial alteration of volcanic glass particles into clays. The thin section work classifies the sample as a tuffaceous sandstone/siltstone.

We believe that the identification of rotary sidewall core sample 10 as volcaniclastics from petrophysics and high mica-content in the XRD work means that the acicular nature of the grain texture seen in the thin-section also indicates a volcaniclastic origin. Like sidewall core sample 31 & 30 we believe the preservation of the acicular character of the volcaniclastics means that the grains have not undergone significant transport distance. We also consider that the apparent lack of transport means the grains were either derived from a single turbidity current event with little or no staging in the hinterland or that they were deposited directly onto the sea-surface through ash-fall and are essentially also 'in-situ'.

Rotary sidewall core 2

Rotary sidewall core sample two was acquired at 1824m MD (Figure 14) and was identified in standard petrophysical interpretation as volcaniclastic but not initially by the image log analysis for reasons that stated above. However, the rotary sidewall core identified the sample as potentially volcaniclastic due to an elevated 'muscovite' percentage in the XRD analysis (Figure 10); in this case the muscovite percentage is only 7% as compared with 31-71% in samples 10, 30 & 31 . This bed lies within the early Messinian.

The thin-section shows that the mineralogy is composed by an alternation of shale with planktonic foraminifera and interlaminations of coarse sift-sized volcanic ash (0.058 mm) (Photo 1 and 2; Figure 14). The glass particles are characterized to be isotropic and angulous in shape. Other minor minerals include detrital quartz, feldspars, and disseminated pyrite. Skeletal components include planktonic foraminifera (globigerinids) occasionally well-preserved or fragmented (Photo 3 and 4: 02). The clays observed probably correspond to zeolites and/or to other clay minerals as alteration products from volcanic glass. The tuff intervals exhibit a good interparticle porosity (Photo 3). The porosity system is associated to a dissolution process of unstable minerals, intra-fossilar spaces (Figure 14, Photos 3 and 4, O3) and microfractures. The sample

exhibits some opened fractures lined by bituminous material (Figure 14, Photos 1 and 2) and other cemented fractures (Figure 14, Photos 3 and 4). Diagenetically the sequence is interpreted as that of sedimentation of volcanic ash particles, burial, compaction, dissolution process and partial alteration of volcanic glass particles into clays. The thin section work classifies the sample as a tuffaceous sandstone/siltstone.

We believe that the identification of rotary sidewall core sample 2 as volcaniclastics from petrophysics and elevated mica-content in the XRD work means that the moderately acicular nature of the grain texture seen in the thin-section also indicates a volcaniclastic origin. However, unlike sample 30, 31 and 10 observe that the preservation of the acicular glass shards is not as good and perhaps this explains the lower mica content evaluation from the XRD work. Given the poorer preservation of acicular shards we speculate that the volcaniclastics grains have undergone more significant transport distance than the other samples, perhaps through multi-phase reworking by turbidity currents or longer staging in the hinterland. We consider that these deposits are not necessarily 'in-situ'.

Relating Cholula-1EXP Volcaniclastics to Onshore Tectonics and Volcanism

When relating the presence of volcaniclastics in the Cholula-1EXP well to the onshore Mexican geology there are a number of factors to consider; the coincidence of the start and finish of the volcanics with the onset and termination of geologic epochs, stages or other sequence boundaries; the coincidence of these onset and termination of the volcaniclastics to changes in structural movement seen offshore and the timing of tectonic events in the onshore; and the linking of the timing of the volcanics in Cholula-1EXP to know volcanic events in the Mexican onshore.

Burdigalian volcaniclastic deposition is restricted to a short interval with three beds totalling 0.9m of volcaniclastics in a 1.6m (Figure 9) interval and do not appear to align with any particular regional sequence boundary or unconformity. As such, it is difficult to identify the absolute ages of these events other than to bracket them within two third order sequence boundaries (Fillon, 2007). Event 8 falls within the LM18.1 sequence (18.10 ma – 20.90 ma), whereas Event 7 falls within the LM16.5 sequence (16.50 ma – 18.10 ma) respectively. Fourteen volcaniclastic beds totalling 4.95m in thickness are identified within the Langhian (Events 5 & 6), notably the first occurrence is directly at Burdigalian/Langhian stage boundary. Eighteen volcaniclastic beds totalling 5.78m in thickness are recorded in the Serravallian (Events 3 & 4); notably the last volcaniclastic deposit is at the just below the significant Middle Miocene unconformity which also includes the base of the lower Tortonian. This boundary would also coincide with a step-change decrease in palaeobathymetry from upper bathyal to outer neritic.

Above this volcaniclastics events are greatly reduced with just two deposits in the Tortonian (Event 2) totalling 0.36m over short interval and do not appear to align with any specific regional sequence boundary or unconformity. Because Event 2 is coincident with the HO of *Discoaster prepentaradius*, we can bracket the absolute age to sometime around 8.30 ma. The last volcaniclastics recorded in Cholula-1EXP are in a single 1.01m bed within the Messinian which also does not appear to align with any specific regional sequence boundary or unconformity although there is a regional condensed section beneath. Unlike Event 2, Event 1 does not have a coincident biostratigraphic datum. At Cholula-1EXP we bracket the age of Event 1 through the identification of the entire range of *Reticulofestra rotaria* (5.94-6.91 ma) a short, but well-defined interval within the NN11c nannofossil subzone (Young et al., 2017).

To attempt to corelate the volcaniclastic events observed in Cholula-1EXP to onshore volcanic episodes onshore Mexico we conducted a literature review for published geochronological data. While not exhaustive, the search revealed data from the Eastern Alkaline Province (Ferrari et al , 2005; Cantagrel et al, 1979), the Los Tuxtlas Volcanic Field (Nelson & Gonzalez-Caver, 1992) and the Trans Mexican Volcanic Belt (Arce et al, 2019; Alva-Valdivia et al, 2000). The data in the literature appears to be sample-biased towards on the Eastern Alkaline Province and the Trans Mexican Volcanic Belt to the west of Cholula-1EXP and so volcanic centres to the south are likely under-represented. The results of age data from these different volcanic events is concatenated into Figure 15 (c.f. Figure 16) in combination with the dates derived from Cholula-1EXP. In this analysis we assume that there is relatively little lag time between the onshore volcanic events and the deposition of the volcaniclastics offshore. In the case of ash-fall deposits directly onto the sea surface this is likely sound though we also believe that even with staging their transport from hinterland to deep-water is close to geologically instantaneous.

The older volcaniclastics in Cholula-1EXP in the Burdigalian to Serravallian (events 3 & 8; Figure 5) – which constitute the bulk of the volcaniclastics - appear to have been derived from Eastern Alkaline Province according to the published data, in particular the Palma Sola Massif. There is the possibility that some of this may be derived from the Trans Mexican Volcanic Belt though this seems of a lower probability. The age span of the Tortonian Event 2 coincides with a single signature and study (Alva-Valdivia et al, 2000) of volcanics in the Guanajuato, Queretaro and Hidalgo regions in the Trans Mexican Volcanic Belt. The youngest volcaniclastic in Cholula-1EXP in the Messinian (Event 1, Figure 5) are possibly derived from both the Eastern Alkaline Province as well as the Trans Mexican Volcanic Belt or combinations thereof. The possibility exists that some material is derived from the Los Tuxtlas Volcanic Field, this possibility might explain the apparent difference in preserved acicular character seen between this and the older events.

We have not attempted to undertake provenance work using mineralogical assemblages as this lies out with the remit of our work. If there are geochronologists who have an interest in doing so we would be interested to discuss the possibility.

Across the Salina del Istmo Basin the Early Miocene is known to vary in thickness from west to east to west though at the more local mini-basin scale the unit appear to be relatively isopachous, the few volcaniclastic Burdigalian deposits seen in Cholula-1EXP fall within this epoch. The Middle Miocene (Langhian-Serravallian) is however marked by significant changes in stratigraphic thicknesses even at the local scale as well as the regional scale, indeed large isopach modification is a recognised character of the Middle Miocene across the Salina del Istmo basin (e.g. Gutiérrez Paredes et al, 2017) resulting from changes in accommodation due to the activation of salt-tectonics. It is this, Middle Miocene epoch, more than any other that is dominated by the presence of volcaniclastics in Cholula-1EXP, with 32 of the 38 volcaniclastic deposits recorded in this interval. The Late Miocene is characterised at the regional scale by thickness variations from east to west but at the local scale returns to a more even distribution akin to the Early Miocene, although still with latent influence of salt-tectonics. As noted above the Late Miocene is relatively devoid of volcaniclastics episodes.

Concentrating on the volcaniclastic dominated interval it is important to note that this Middle Miocene period records the onset of the several tectonic events that affect the southern Gulf of Mexico; the Chiapanecan Orogeny, Chiapanecan Deformation phase and Salina del Istmo salt tectonics (as well as the Mexican Ridges in Western Mexico). We contend that that the volcaniclastics seen in the Cholula-1EXP well is a result of compression onshore at the onset of the Chiapanecan Orogeny, resulting from the subduction of the Cocos Plate beneath the North

American plate (Gutiérrez-Paredes et al, 2018) and we speculate that the presence of the volcaniclastics relate to volcanic activity that resulted from this subduction event.

Implications for Hydrocarbon Prospectivity

Volcaniclastics, a relatively uncommon facies, with unusual mineralogical, petrophysical and geophysical properties present unique recognition challenges as well as opportunities. In terms of recognition we note during the period of investigation that several initial characterisations had to be modified as data emerged. Starting at the small-scale initial laboratory analysis through the XRD work identified as “mica” and was later re-classified as volcanic glass in the light of the thin section descriptions. Petrophysically when Cholula-1EXP was logged, initially we observed low density, high resistivity beds in the Middle Miocene and older. These looked like potential pay sands and Murphy attempted MDT pressures in these zones which all proved to be tight. Following acquired sidewall cores in some of the ‘sands’ of them we observed they were all volcanic ash beds and calculations were modified accordingly. Similarly, in the image log analysis some initial interpretation had to be overturned. For event 2 in the Tortonian the image-log did not initially identify the beds at 2020m as volcaniclastics. The image log did show a similar borehole response to the other volcaniclastics but didn’t have the characteristic log or CPI response and were associated with a small-scale fault which resulted in poor image quality, so they were initially classified as thin massive sandstones. For event 1 in the Messinian the volcaniclastic bed was a more isolated, more resistive, and thicker bed (~1 m) in comparison to other volcaniclastic beds, which showed relatively poor image quality and limited resistivity contrast and that is enclosed within thick mudrocks. RSWC 2 indicates that in fact it is a thick and isolated volcanic deposit likely associated to an exceptional explosive volcanic event.

Distortion of AVO character / False positives while not impacting Cholula-1EXP specifically we note from the literature that ash-bearing intervals are recognizable on seismic and occur as locally bright reflections which may mimic depositional features. Finally, we note that while other negatives include poor reservoir quality due to the presence of textually immature volcaniclastics material within sands in one sand in Cholula-1EXP one such volcaniclastics is actually a hydrocarbon pay zone.

On the positive scale the presence of volcaniclastics, particularly within the Middle Miocene presents an extra level of opportunity for regional correlation when used in conjunction with standard biostratigraphy or indeed as tephrochronologic markers in their own right. Indeed, in an exploration setting within the Salina del Istmo Basin the increased presence of volcanics while drilling may present an early indicator of having entered, or having drilled through, Middle Miocene strata.

Acknowledgements

The authors would like to acknowledge our partners in Block 5, Petronas and Wintershall Dea as well as Murphy management and the Comisión Nacional de Hidrocarburos for permission to publish this data and interpretation. We would also like to thank all service providers involved in the drilling of Cholula-1EXP and in the subsequent post-drill analysis, particularly Weatherford Labs for their work on the side-wall cores. Finally, we would like to acknowledge the hard work and dedication of all team members of the Murphy Mexico exploration team and counterparts in our partners past and present. Dedicated to Edna & Eric Smith.

References

Ángeles-Aquino, F., Reyes-Núñez, Quesada- Muñeton and Meneses Rocha, J.J., 1994.Tectonic Evolution, Structural Styles and Oil habitat in Campeche sound, Mexico: Gulf Coast Association of Geological Societies Transactions. V 44, pp 53-62.

Arce, J.L., Layer, P.W., Macías, J.L., Morales-Casique, E., García-Palomo, A., Jiménez-Domínguez, F.J., Benowitz, J., Vásquez-Serrano, A., 2019. Geology and stratigraphy of the Mexico Basin (Mexico City), central Trans-Mexican Volcanic Belt. Journal of Maps 15, 320–332. https://doi.org/10.1080/17445647.2019.1593251

Alva-Valdivia, L.M., Goguitchaichvili, A., Ferrari, L., Rosas-Elguera, J., Urrutia-Fucugauchi, J., Zamorano-Orozco, J.J., 2000. Paleomagnetic data from the Trans-Mexican Volcanic Belt: implications for tectonics and volcanic stratigraphy. Earth Planet Sp 52, 467–478. https://doi.org/10.1186/BF03351651

Burley, S.D., Breitfeld, H.T., Stanbrook, D.A., Morley, R.J., Kassan, J., Sukarno, M., Wantoro, D.W., 2020 (in press). A tuffaceous volcaniclastic turbidite bed of Early Miocene age in the Temburong Formation of Labuan, NW Borneo and its implications for the Proto-South China Sea subduction in the Burdigalian. The Depositional Record, v6.

Buffler, R.T., and Sawyer D.S., 1985. Distribution of crust and early history Gulf of Mexico Basin. Gulf Coast Association of Geological Societies Transactions.35.333-344.

Cantagrel, J.-M., Robin, C., 1979. K-Ar dating on Eastern Mexican volcanic rocks -relations between the andesitic and the alkaline provinces. Journal of Volcanology and Geothermal Research 5, 99–114.

Clare, M.A., Le Bas, T., Price, D.M., Hunt, J.E., Sear, D., Cartigny, M.J.B., Vellinga, A., Symons, W., Firth, C., Cronin, S., 2018. Complex and Cascading Triggering of Submarine Landslides and Turbidity Currents at Volcanic Islands Revealed from Integration of High-Resolution Onshore and Offshore Surveys. Front. Earth Sci. 6, 223. https://doi.org/10.3389/feart.2018.00223

Ferrari, L., Tagami, T., Eguchi, M., Orozco-Esquivel, Ma.T., Petrone, C.M., Jacobo-Albarrán, J., López-Martínez, M., 2005. Geology, geochronology and tectonic setting of late Cenozoic volcanism along the southwestern Gulf of Mexico: The Eastern Alkaline Province revisited. Journal of Volcanology and Geothermal Research 146, 284–306. https://doi.org/10.1016/j.jvolgeores.2005.02.004

Fillon, Richard H, 2007. 2007 Gulf of Mexico basin chronostratigraphic database. Earth Studies Group, New Orleans, Louisiana

Gradstein, F.M., Ogg, J.G., Schmitz, M.D., and Ogg, G.M., eds, 2012, The Geological Time Scale 2012, Amsterdam, Elsevier, 2 vols., 1144 p

Friedman, B., 2006. Ash Deposits Can be Deceiving. AAPG Explorer 28–31.

Gutiérrez Paredes, H.C., Martinez Medrano, M., Sessarego, H.L., 2009. Chapter 18: Provenance for the Middle and Upper Miocene Sandstones of the Veracruz Basin, Mexico, *in*: Bartolini, C., Ramos, R.J.R. (Eds.), Petroleum Systems in the Southern Gulf of Mexico, AAPG Memoir. pp. 397–407.

Gutiérrez Paredes, H.C., Catuneanu, O., Hernández Romano, U., 2017. Sequence stratigraphy of the Miocene section, southern Gulf of Mexico. Marine and Petroleum Geology 86, 711–732. https://doi.org/10.1016/j.marpetgeo.2017.06.022

Hernández, H.S., 2013. Stratigraphic characterization and evolution of a Mid-Tertiary age deep water system, Holok area, SW Gulf of Mexico (PhD). University of Aberdeen, Aberdeen, UK.

Nelson, S.A., Gonzalez-Caver, E., 1992. Geology and K-Ar dating of the Tuxtla Volcanic Field, Veracruz, Mexico. Bull Volcanol 55, 85–96. https://doi.org/10.1007/BF00301122

Padilla y Sánchez, R.J., 2007. Evolución geológica del Sureste Mexicano desde el Mesozoico al presente en el contexto regional del Golfo de México. Boletín de la Sociedad Geológica Mexicana 59, 19–42.

Sanchez Montes de Oca, R. (2006), Curso Cuenca del Sureste, report, 296pp., Petrol. Mex., Mexico City.

Task Fronterra Geoscience, 2019. Well: Cholula-1EXPEXP Block 5 Gulf of Mexico (offshore Mexico). Structural and sedimentological interpretation of Schlumberger Quanta Geo image log data (Murphy Proprietary Report No. HD0419- 014).

Totten, J., Hanan, H., Jurik, M.A., 2005. The Occurrence and Seismic Expression of Volcanic Ash Beds in the Gulf of Mexico. GCAGS Transactions 55, 810–820.

Young, J.R., Bown P.R., Lees J.A. (2017) Nannotax3 website. International Nannoplankton Association. Accessed 21 Apr. 2017. URL: http://www.mikrotax.org/Nannotax3

Click to View Poster

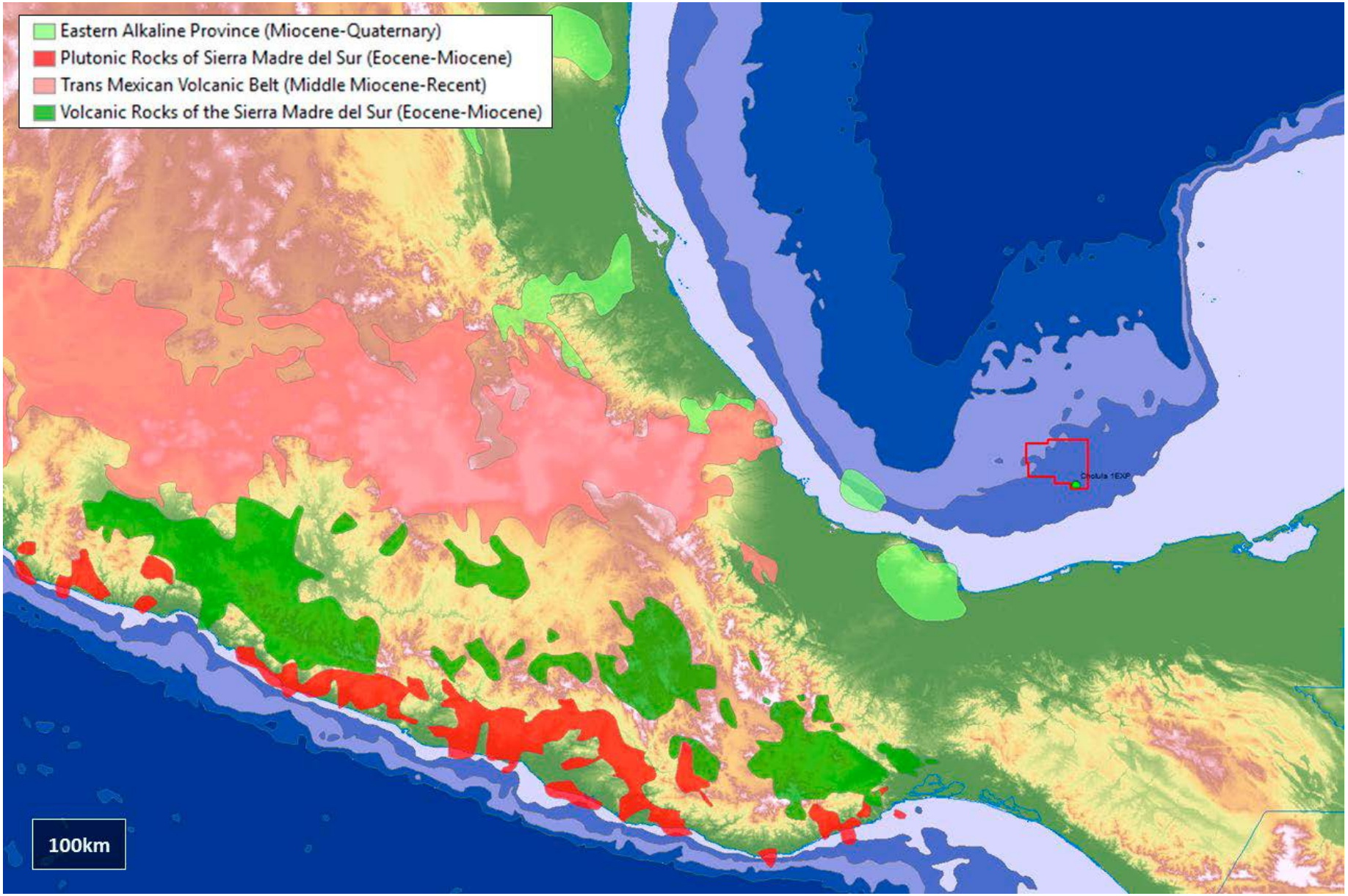

Figure 1. Main volcanic provinces active during the Miocene and regional setting of the Cholula-1EXP exploration well within Block 5 (red outline). Blue shade represents present-day bathymetry.

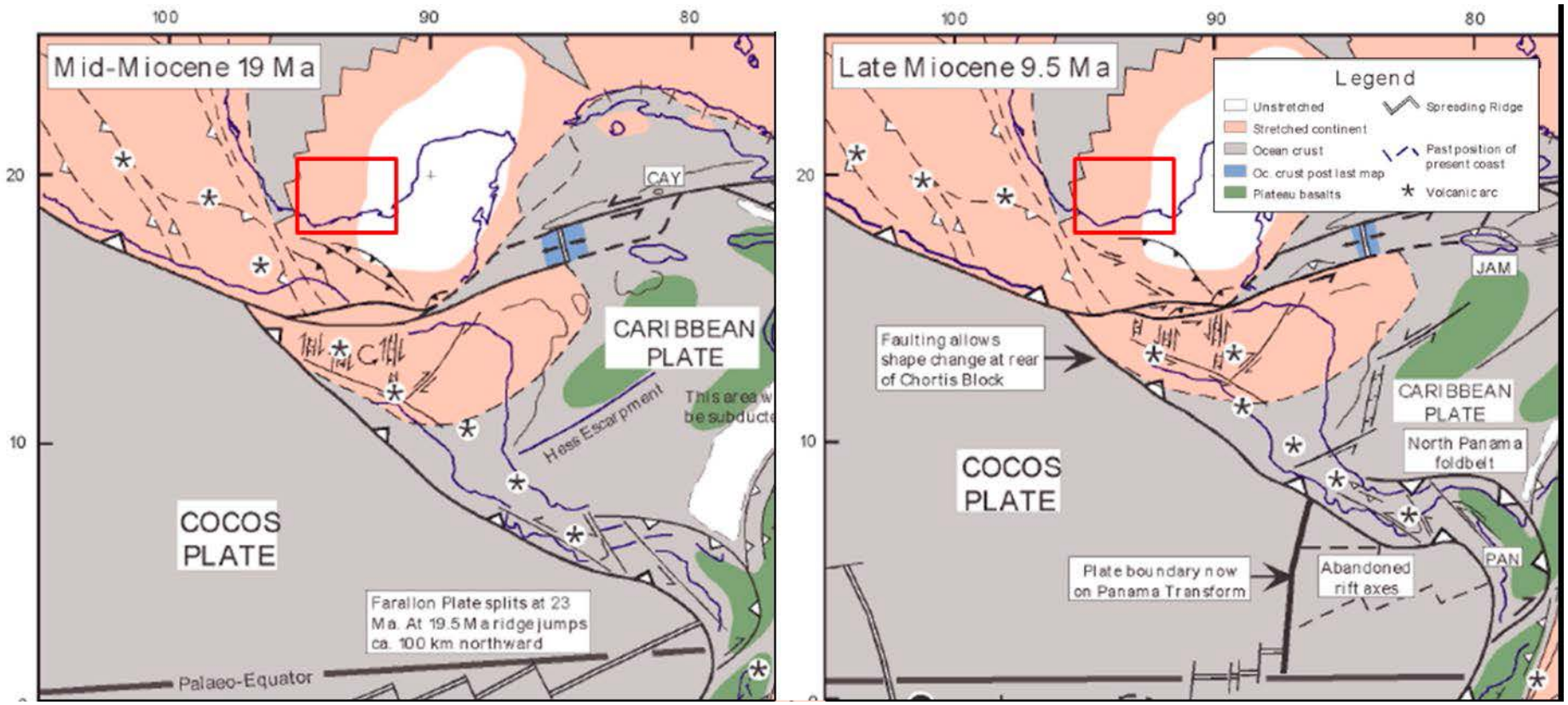

Figure 2. Mid Miocene to Late Miocene plate reconstruction modified from Pindell & Kennan (2001). CAY = Cayman Trough, JAM = Jamaica, PAN = Panama Trench.

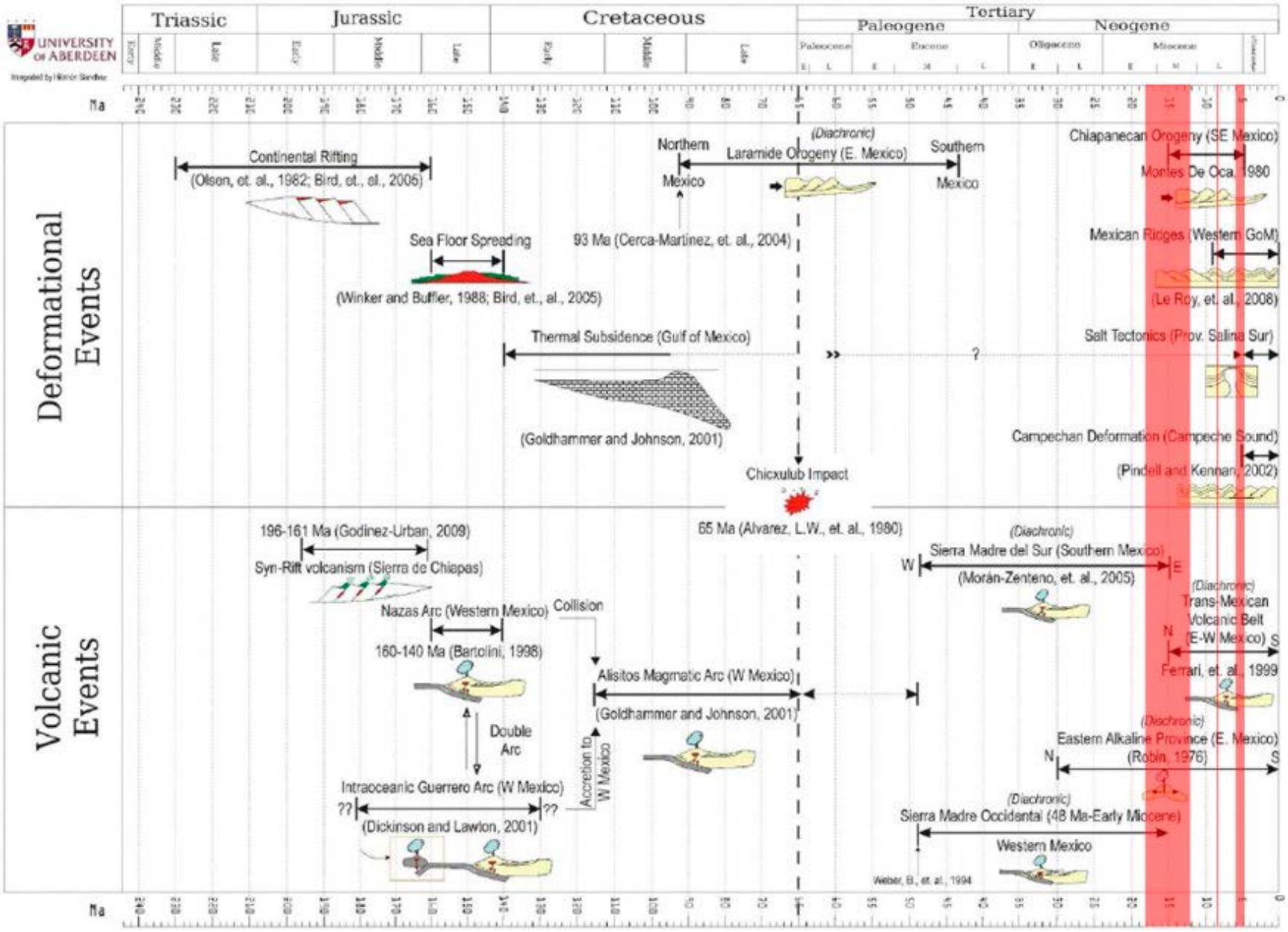

Figure 3. Key volcanic and deformation events in the Gulf of Mexico (Hernández, 2013), red bars indicate timing of volcaniclastic beds observed in Cholula-1EXP.

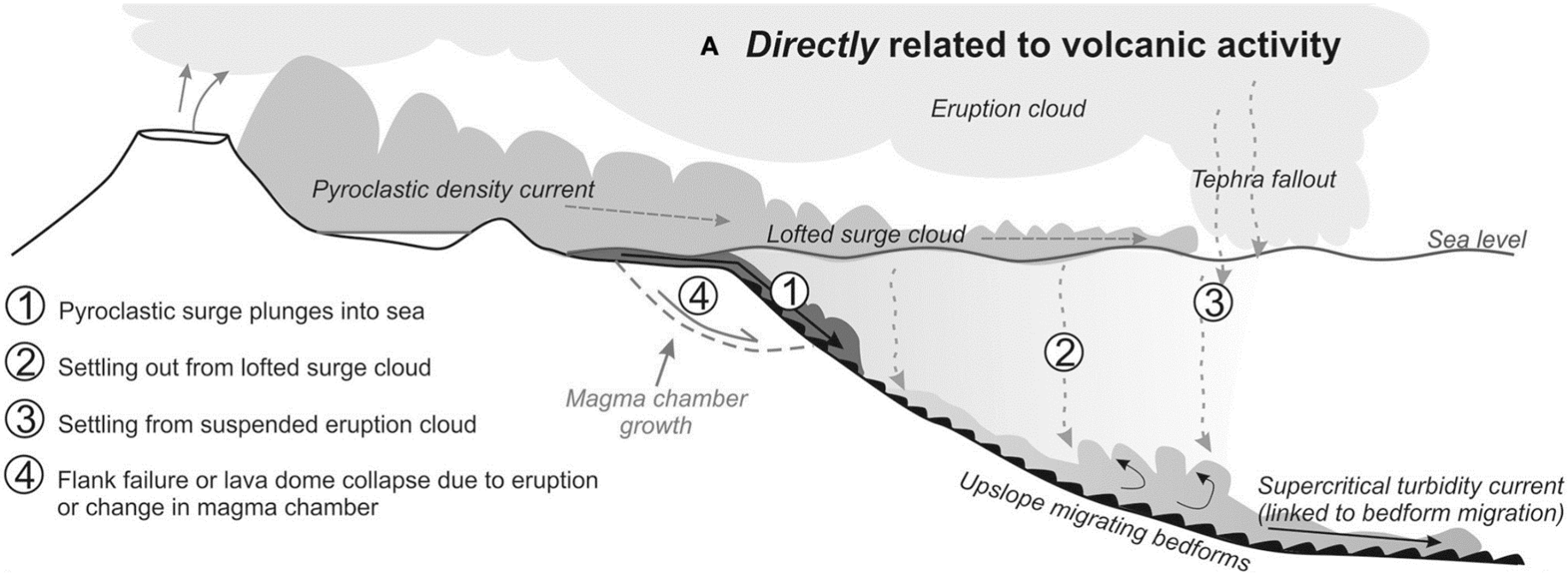

Figure 4. Summary relationships between onshore and deep-water volcaniclastic sedimentary processes (Clare et al, 2018).

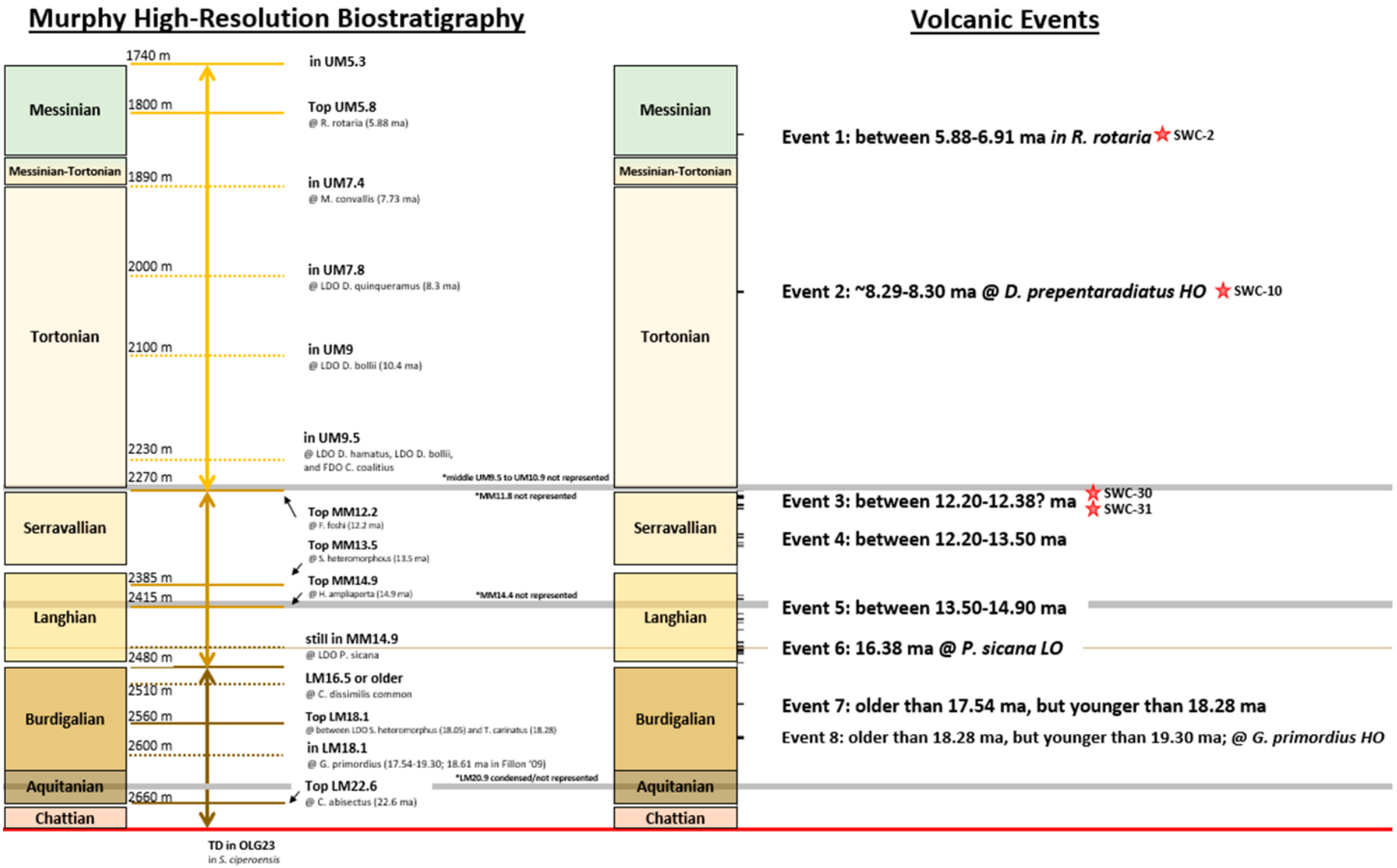

Figure 5. Stratigraphy, biostratigraphy and chronostratigraphy of Cholula-1EXP. Murphy in-house sequences from Fillon (2007). HO = Highest Occurrence, LO = Lowest Occurrence. Numerical ages are calibrated to Geological Time Scale (Gradstein et al, 2012)

a

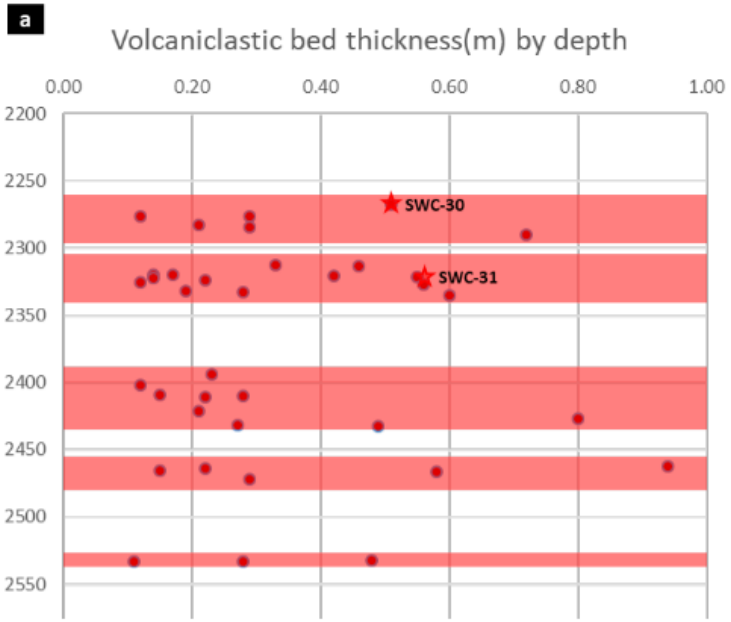

b

Age	Number of tuff layers	Minimum Thickness (m)	Maximum Thickness (m)	Mean Thickness (m)	Total Thickness (m)
Messinian	1	1.01	1.01	1.01	1.01
Tortonian	2	0.16	0.20	0.18	0.36
Serravallian	18	0.12	0.72	0.32	5.78
Langhian	14	0.12	0.94	0.35	4.95
Burdigalian	3	0.11	0.48	0.29	0.87

Figure 6. Distribution of ash beds. a) ash-bed thickness within the interpreted image log interval as a function of depth. b) table showing distribution of ash bed thicknesses by stratigraphic age. 32 of the 38 volcaniclastic deposits recorded occur within the Middle Miocene. Data derived by Task Fronterra Geoscience, 2019.

a

	Quartz	Orthoclase K	Albite Na	Wet Cl/Sh 1	X FreeW	OBM Filtrate	U Oil	U FreeW	Units
RHOB	2.65	2.57	2.61	2.27	1.155	1	0	0	G/C3
NPHIL	-0.04	-0.006	-0.005	0.4	0.8881	1	0	0	V/V
THOR	2	3	1	15	0	0	0	0	PPM
POTA	0	10.21	0	8	0	0	0	0	%
CT	0	0	0	1.111	0	0	0	40	MH/M

b

	Quartz	Orthoclase K	Albite Na	Spec Min2	Wet Cl/Sh 1	X FreeW	OBM Filtrate	U Oil	U FreeW	Units
RHOB	2.65	2.57	2.61	1.65	2.27	1.155	1	0	0	G/C3
NPHIL	-0.04	-0.006	-0.005	0.6	0.4	0.8881	1	0	0	V/V
THOR	2	3	1	15	15	0	0	0	0	PPM
POTA	0	10.21	0	2.5	8	0	0	0	0	%
CT	0	0	0	0	1.111	0	0	0	40	MH/M

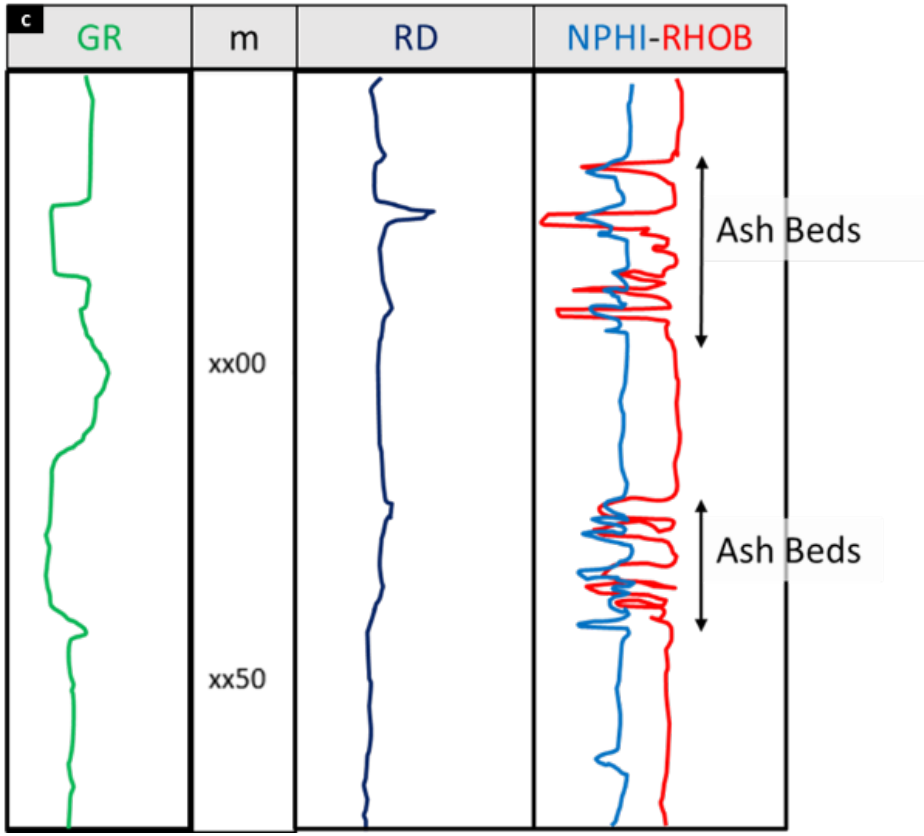

Figure 7. Petrophysical analysis tables a and b and schematic representation of volcanic ash log motif (c). See text for discussion.

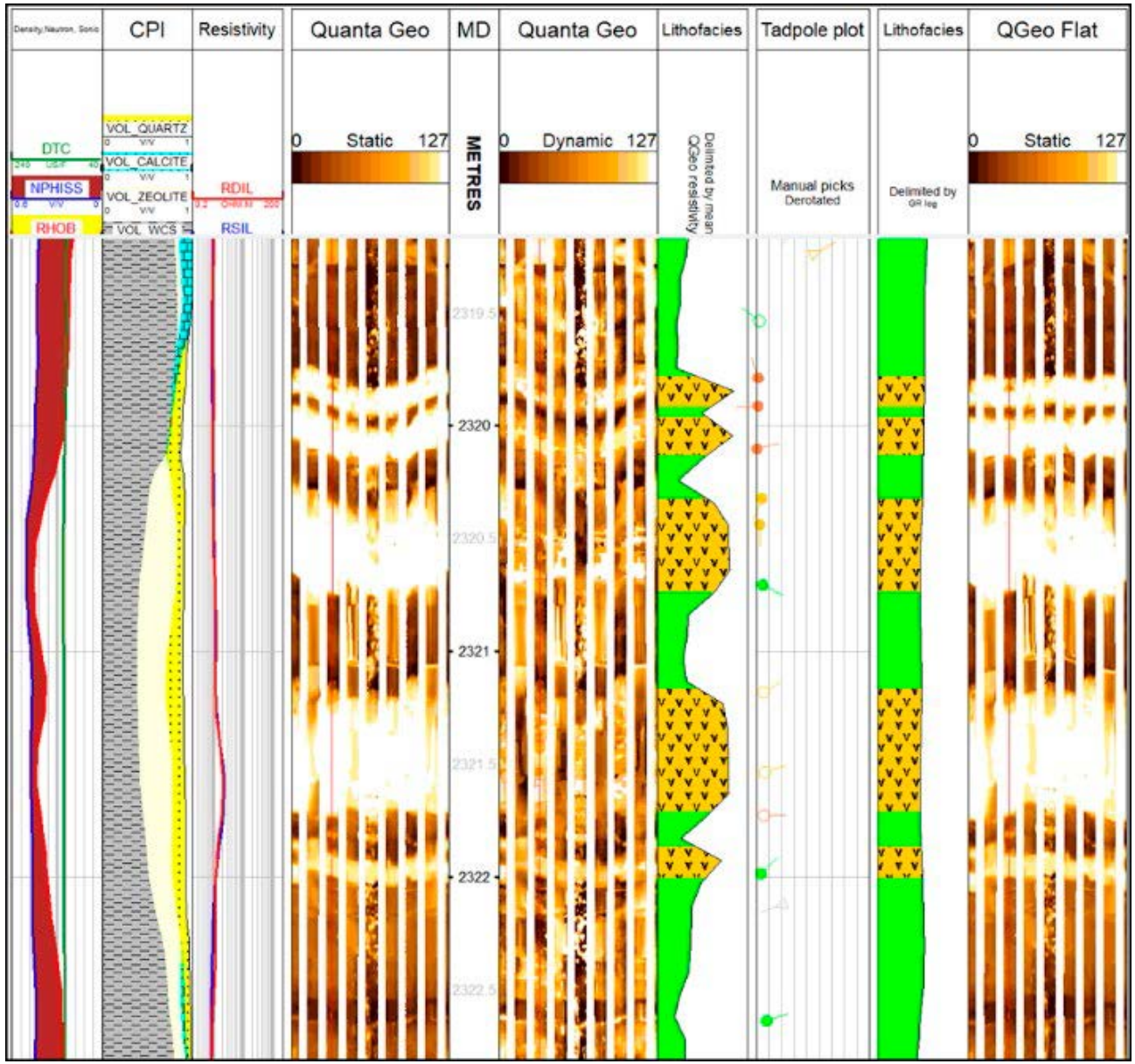

Figure 8. Image log character of volcaniclastic layers in Serravallian sediments (interval 2319.5-2324.5 m) showing background mud drape deposits punctuated by isolated and relatively thick volcanic tuffs, with a characteristic log response. The basal thicker layer corresponds to rotary sidewall cores #30/31. Task Fronterra Geoscience, 2019.

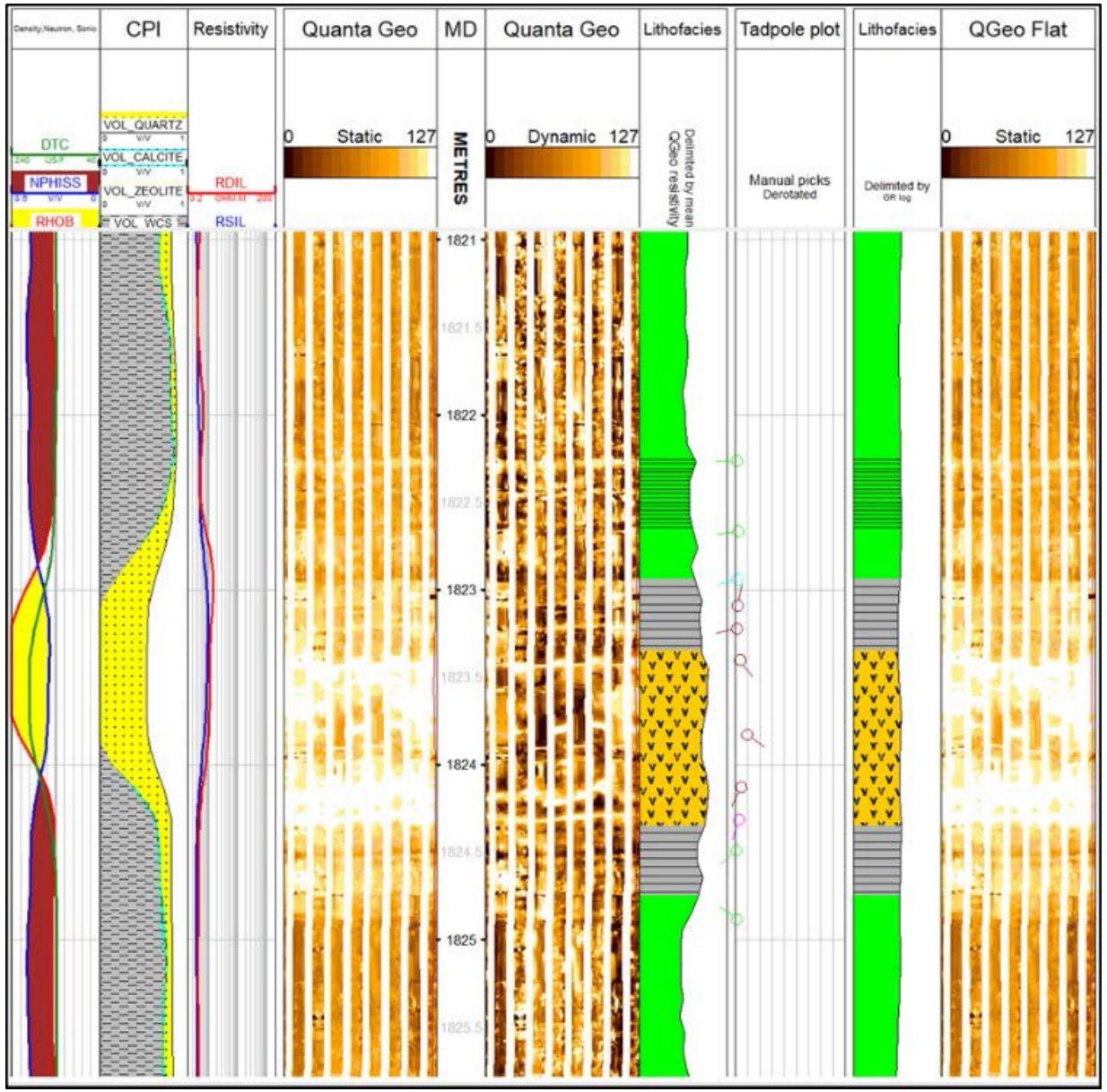

Figure 9. Image log character of a thick volcanic tuff layer identified toward the base of the Messinian, which is enclosed in stratified to massive mudstones. This ash bed was sampled by rotary sidewall core #2 and represents the last episode of volcaniclastic deposition recorded in Cholula-1EXP study interval. Task Fronterra Geoscience, 2019.

	Depth	Clays					Carbonates				Other Minerals								Totals		
	Top	Glauconite	Chlorite	Kaolinite	Ilite/Mica	Mx I/S*	Calcite	Dolomite	Ankerite	Siderite	Quartz	K-feldspar	Plagioclase	Pyrite	Apatite	Gypsum	Muscovite	Anhydrite	Clays	Carbonates	Others
SWC02	1824	1	2	0	12	24	1	0	0	1	14	3	28	7	Tr	0	7	0	39	2	59
SWC03	1924	1	2	0	9	9	9	0	0	2	33	7	26	1	1	0	0	0	21	11	68
SWC05	1973	2	4	6	4	8	5	0	2	0	22	17	29	1	0	0	0	Tr	24	7	69
SWC07	2004	2	2	8	2	5	1	1	1	0	19	25	28	3	0	0	3	0	19	3	78
SWC08	2010	0	4	11	6	27	14	1	0	0	18	3	13	1	0	0	2	0	48	15	37
SWC09	2016	2	Tr	0	1	3	1	1	0	0	23	34	34	1	0	0	0	0	6	2	92
SWC10	2020	1	Tr	0	Tr	4	4	0	0	0	6	8	5	1	0	0	71	0	5	4	91
SWC11	2033	2	Tr	2	5	39	7	2	0	Tr	19	3	17	1	2	0	1	0	48	9	43
SWC12	2048	3	5	7	4	20	13	Tr	0	0	19	2	22	2	Tr	1	2	0	39	13	48
SWC14	2103	2	0	3	4	24	8	1	0	0	21	11	19	4	1	0	2	0	33	9	58
SWC15	2105	2	2	0	7	33	11	1	0	Tr	22	4	13	3	0	1	1	0	44	12	44
SWC16	2113	3	12	5	9	29	5	1	0	0	17	4	12	1	Tr	0	2	0	58	6	36
SWC17	2116	2	2	0	3	19	5	5	0	0	29	3	29	2	Tr	Tr	1	0	26	10	64
SWC18	2124	2	3	3	8	26	7	3	0	0	21	3	21	1	1	0	1	0	42	10	48
SWC19	2138	2	0	2	1	16	10	7	0	0	30	3	26	1	2	0	0	0	21	17	62
SWC20	2174	2	0	1	1	9	2	9	0	0	21	2	48	4	0	0	1	0	13	11	76
SWC21	2180	3	0	5	4	35	15	1	0	0	21	2	11	2	0	Tr	1	0	47	16	37
SWC22	2185	1	1	0	2	9	3	3	0	0	34	6	38	1	1	0	1	0	13	6	81
SWC23	2197	2	2	0	4	19	3	2	0	0	23	18	23	2	0	Tr	2	0	27	5	68
SWC24	2204	2	0	2	1	7	7	3	0	0	36	6	31	4	0	0	1	0	12	10	78
SWC25	2220	2	0	7	2	10	4	1	0	0	25	3	43	Tr	2	0	1	0	21	5	74
SWC26	2225	3	1	3	1	3	2	2	0	0	26	14	41	2	0	0	2	0	11	4	85
SWC27	2235	3	2	7	4	16	7	1	0	0	21	14	23	1	1	0	0	0	32	8	60
SWC28	2245	1	1	0	4	15	7	3	0	0	27	9	31	2	Tr	Tr	0	0	21	10	69
SWC29	2257	3	5	0	9	40	9	1	0	0	19	4	9	1	Tr	0	0	0	57	10	33
SWC30	2267	3	1	0	4	22	3	2	0	0	6	6	21	1	0	0	31	0	30	5	65
SWC31	2321	7	Tr	0	1	3	17	1	0	0	13	5	8	3	0	0	42	0	11	18	71
SWC32	2372	1	4	0	5	25	30	2	0	0	15	6	11	Tr	0	0	1	0	35	32	33
SWC33	2425	1	3	0	9	34	23	1	0	0	17	3	8	1	0	0	0	0	47	24	29
SWC34	2476	2	4	8	6	29	19	1	0	0	16	3	10	1	0	0	1	0	49	20	31

Figure 10. Tabulated mineralogical analysis from Cholula-1EXP rotary sidewall cores. Note the anomalously high percentages of muscovite mica reported for cores 10, 30 & 31 and the more modestly elevated levels in core 2. Tr=Trace.

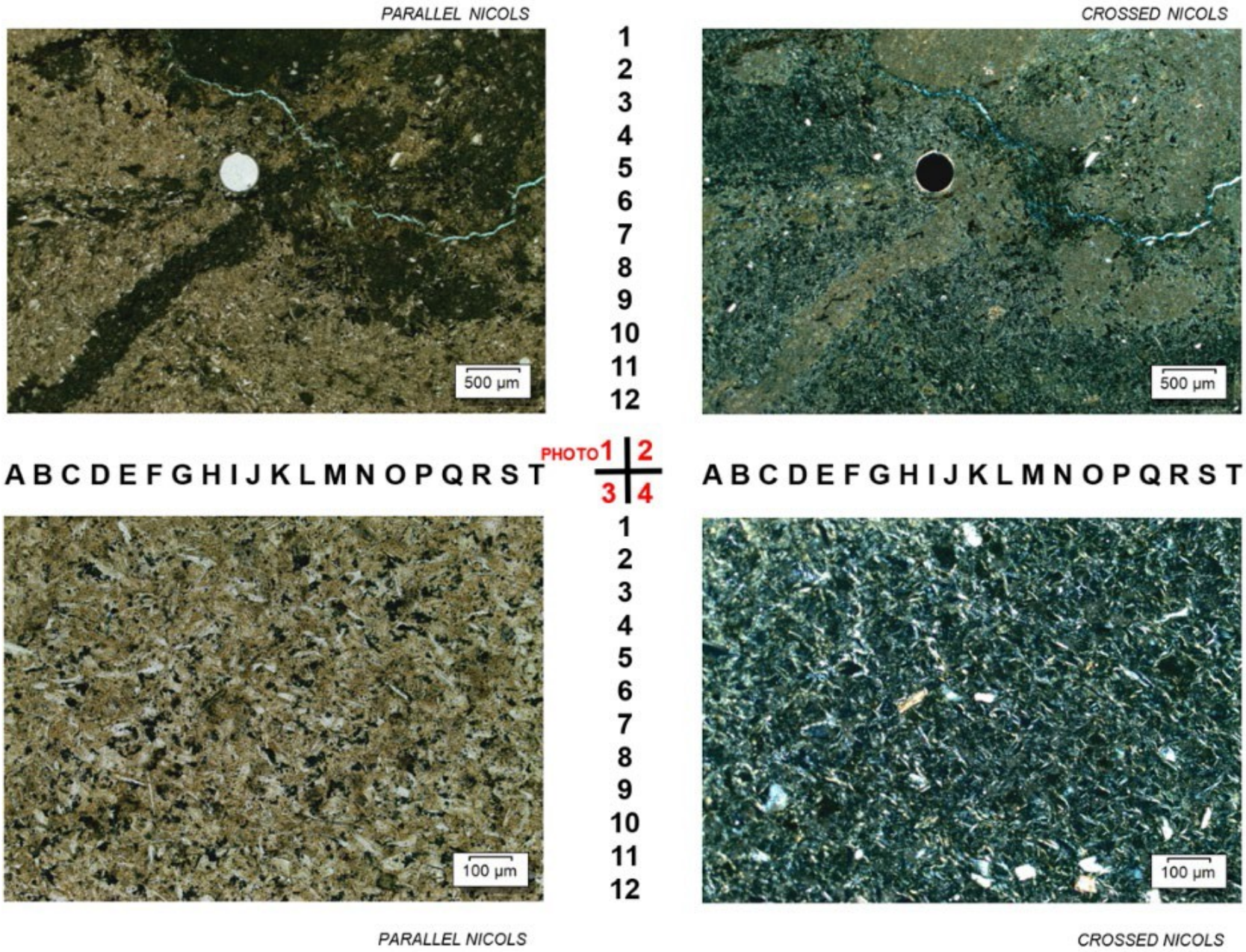

Figure 11. Thin-section microphotographs for rotary side wall core #31. See text for discussion.

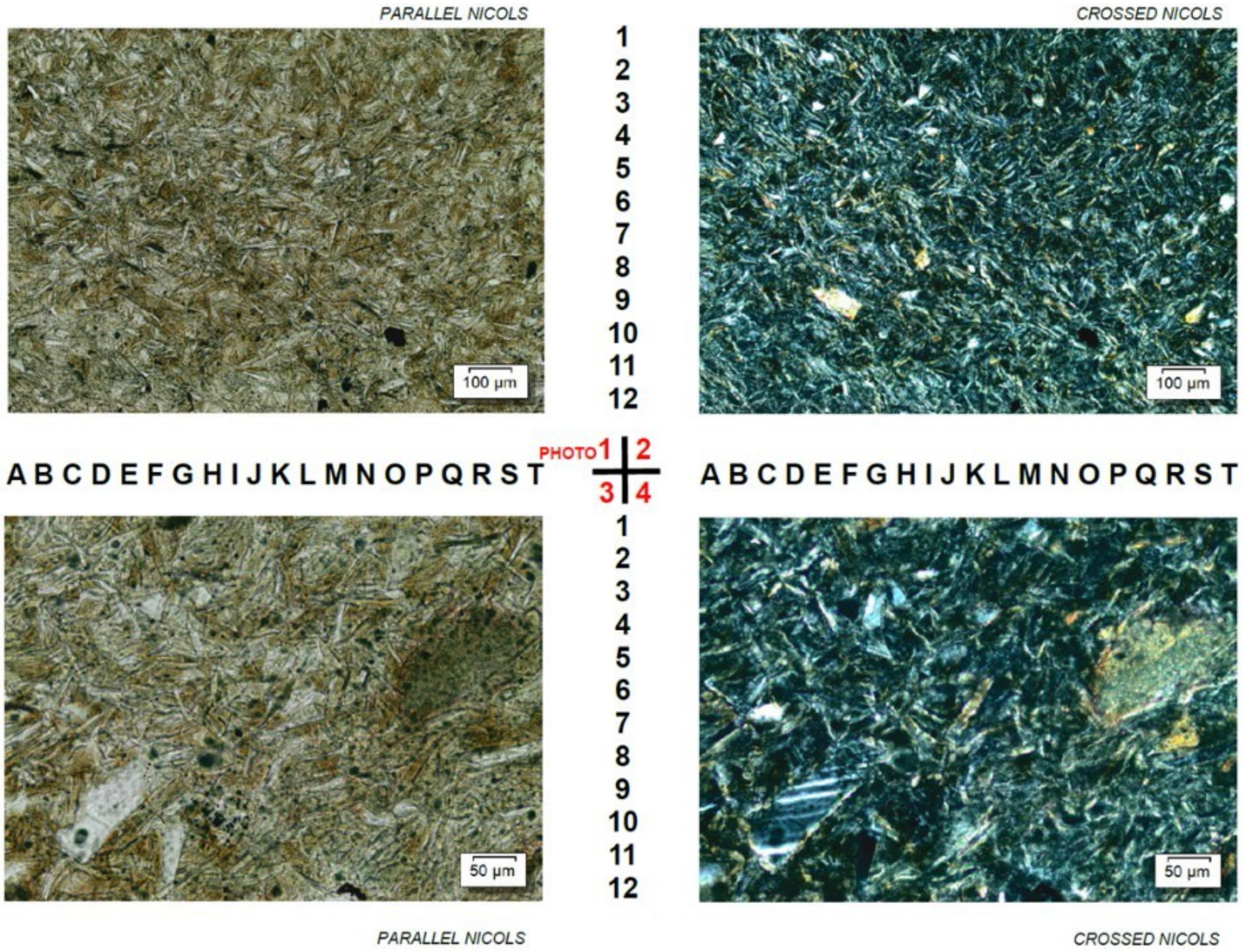

Figure 12. Thin-section microphotographs for rotary side wall core #30. See text for discussion.

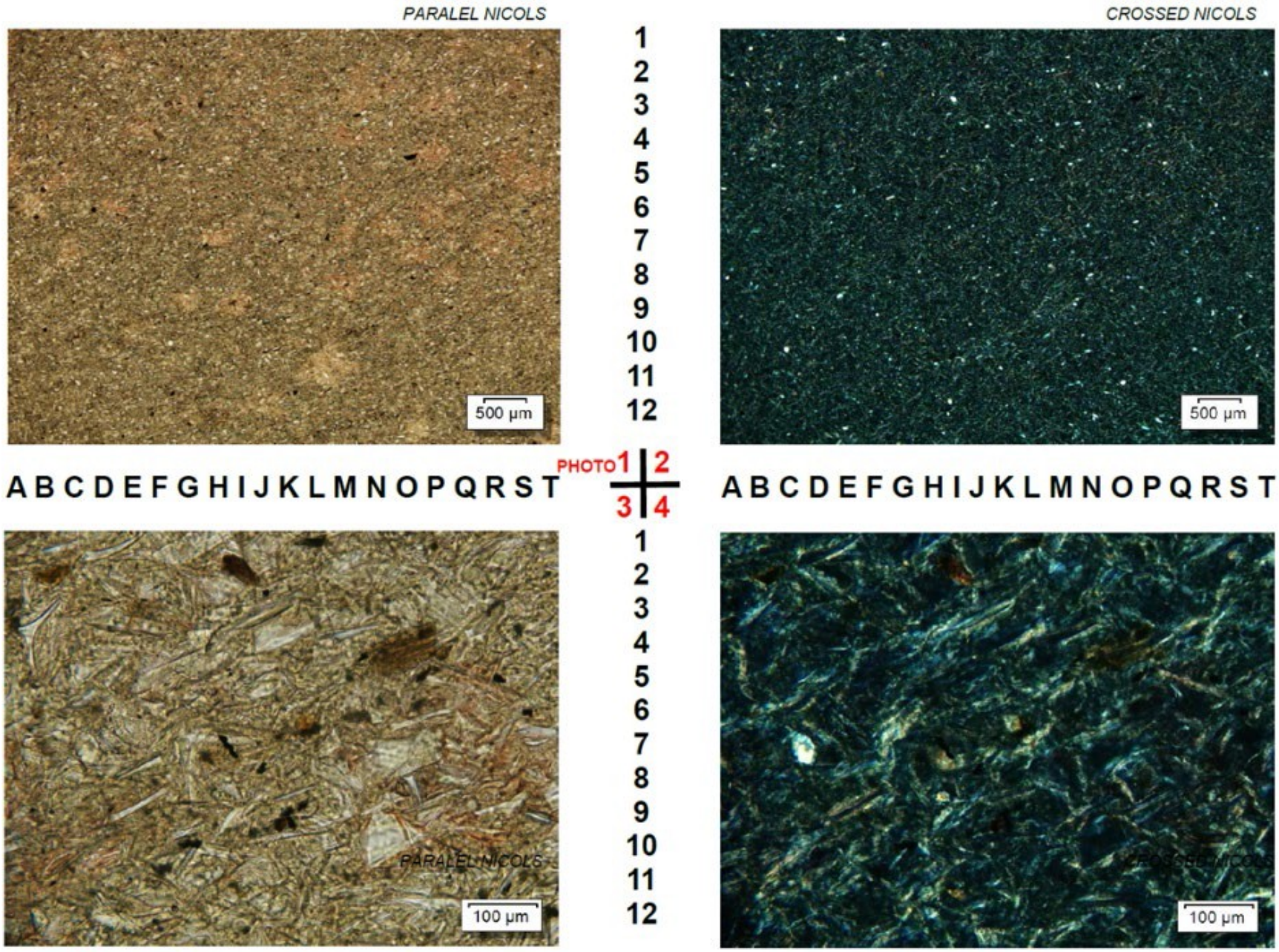

Figure 13. Thin-section microphotographs for rotary side wall core #10. See text for discussion.

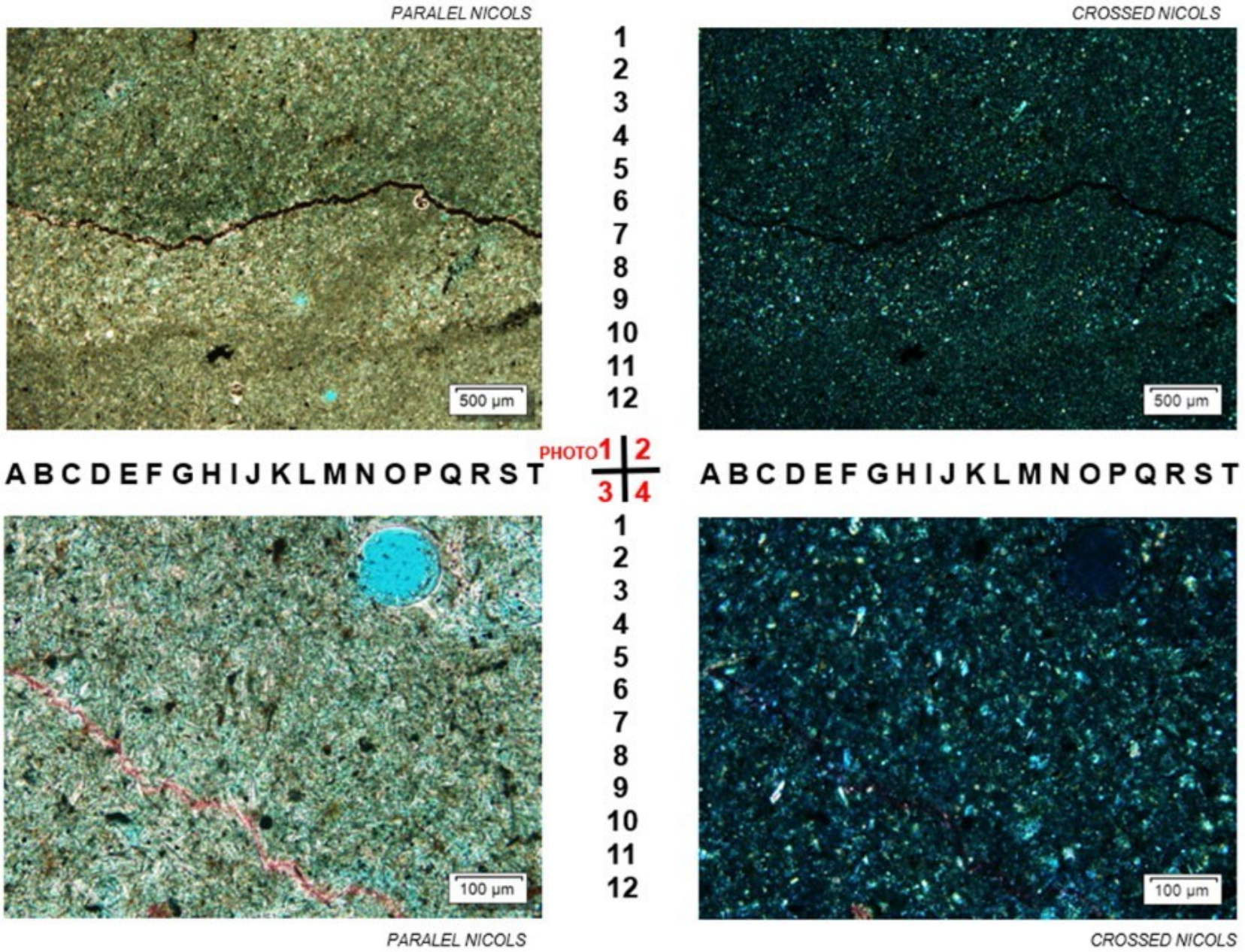

Figure 14. Thin-section microphotographs for rotary side wall core #2. See text for discussion.

Age (Ma)	Age Error (Ma)	Age Min (Ma)	Age Max (Ma)	Sub-region	Region	Publication	Cholula-1EXP
4.6	0.2	4.4	4.8	Southern Hidalgo	EAP/TMVB	4	
4.7	0.1	4.6	4.8	Rio Grande de Santiago (Guadalajara)	TMVB	2	
5.2	0.3	4.9	5.4	Southern Hidalgo	EAP/TMVB	4	
5.7	0.1	5.6	5.9	Tlanchinol flows	EAP	3	1
6.0	0.3	5.7	6.2	Southern Hidalgo	EAP/TMVB	4	1
6.5	0.2	6.3	6.7	Palma Sola massif (inclusive the Miocene calc-alkaline rocks)	EAP	4	1
6.5	0.3	6.2	6.8	Northern Hidalgo	EAP/TMVB	4	1
6.6	0.1	6.5	6.7	Alamo volcanic field and Sierra de Tantima	EAP	3	1
6.7	0.1	6.5	6.8	Alamo volcanic field and Sierra de Tantima	EAP	3	1
6.7	0.4	6.3	7.1	Alamo volcanic field and Sierra de Tantima	EAP	3	1
6.7	0.1	6.6	6.9	Alamo volcanic field and Sierra de Tantima	EAP	3	1
6.8	0.1	6.7	6.8	Alamo volcanic field and Sierra de Tantima	EAP	3	1
6.9	0.8	6.1	7.7		LTVF	5	1
6.9	0.1	6.8	7.0	Alamo volcanic field and Sierra de Tantima	EAP	3	1
6.9	0.2	6.8	7.1	Chiconquiaco–Palma Sola area	EAP	3	1
7.0	0.2	6.8	7.2	Sierra de Tamaulipas	EAP	4	1
7.0	0.2	6.9	7.2	Alamo volcanic field and Sierra de Tantima	EAP	3	1
7.1	0.3	6.8	7.4	Northern Hidalgo	EAP/TMVB	4	1
7.1	0.2	7.0	7.3	Alamo volcanic field and Sierra de Tantima	EAP	3	
7.1	0.1	7.0	7.3	Alamo volcanic field and Sierra de Tantima	EAP	3	
7.1	0.1	7.0	7.3	Alamo volcanic field and Sierra de Tantima	EAP	3	
7.3	0.1	7.2	7.4	Tlanchinol flows	EAP	3	
7.3	0.2	7.2	7.5	Alamo volcanic field and Sierra de Tantima	EAP	3	
7.3	0.1	7.2	7.5	Alamo volcanic field and Sierra de Tantima	EAP	3	
7.3	0.1	7.2	7.5	Tlanchinol flows	EAP	3	
7.4	0.6	6.8	8.0	Northern Hidalgo	EAP/TMVB	4	
7.5	0.1	7.4	7.6	Chiconquiaco–Palma Sola area	EAP	3	
7.6	0.2	7.4	7.7	Alamo volcanic field and Sierra de Tantima	EAP	3	
7.7	0.3	7.4	8.0	South (Miocene and trans-Mexican neovolcanic belt)	TMVB	4	
8.1	0.8	7.3	8.9	Guanajuato, Queretaro and Hidalgo	TMVB	2	2
8.5	0.5	8.0	9.0	Guanajuato, Queretaro and Hidalgo	TMVB	2	2
8.5	0.5	8.0	9.0	Guanajuato, Queretaro and Hidalgo	TMVB	2	2
8.5	0.5	8.0	9.0	Guanajuato, Queretaro and Hidalgo	TMVB	2	2
8.5	0.5	8.0	9.0	Guanajuato, Queretaro and Hidalgo	TMVB	2	2
8.7	1.0	7.7	9.7	Los Altos de Jalisco	TMVB	2	
9.0	0.3	8.7	9.3	North ("Atotonilco el Grande" sequence and Zimapan volcanics)	TMVB	4	
9.0	0.2	8.9	9.2	Alamo volcanic field and Sierra de Tantima	EAP	3	
9.3	0.3	9.0	9.5	Rio Grande de Santiago (Guadalajara)	TMVB	2	
9.3	0.3	9.0	9.5	Rio Grande de Santiago (Guadalajara)	TMVB	2	
9.3	0.3	9.0	9.5	Rio Grande de Santiago (Guadalajara)	TMVB	2	
9.3	0.3	9.0	9.5	Rio Grande de Santiago (Guadalajara)	TMVB	2	
9.4	0.5	8.9	9.9	Guanajuato, Queretaro and Hidalgo	TMVB	2	
9.4	0.5	8.9	9.9	Guanajuato, Queretaro and Hidalgo	TMVB	2	
9.4	0.5	8.9	9.9	Guanajuato, Queretaro and Hidalgo	TMVB	2	
9.6	1.0	8.6	10.6	Guanajuato, Queretaro and Hidalgo	TMVB	2	
10.1	0.4	9.7	10.5	Los Altos de Jalisco	TMVB	2	
10.2	0.1	10.1	10.3	Guanajuato, Queretaro and Hidalgo	TMVB	2	
10.2	0.3	9.9	10.5	Los Altos de Jalisco	TMVB	2	
10.2	0.3	9.9	10.6	Rio Grande de Santiago (Guadalajara)	TMVB	2	
10.3	0.8	9.4	11.1	Rio Grande de Santiago (Guadalajara)	TMVB	2	
10.3	0.5	9.8	10.8	Los Altos de Jalisco	TMVB	2	
10.5	0.4	10.1	10.9	Los Altos de Jalisco	TMVB	2	
10.5	0.5	10.0	11.0	Rio Grande de Santiago (Guadalajara)	TMVB	2	
11.0	0.2	10.8	11.2	Rio Grande de Santiago (Guadalajara)	TMVB	2	
11.0	0.2	10.8	11.2	Rio Grande de Santiago (Guadalajara)	TMVB	2	
11.0	2.0	9.0	13.0	Los Altos de Jalisco	TMVB	2	
11.1	0.2	10.9	11.3	Chiconquiaco–Palma Sola area	EAP	3	
12.0	2.0	10.0	14.0	Los Altos de Jalisco	TMVB	2	
13.5	1.3	12.2	14.8	Los Altos de Jalisco	TMVB	2	3/4
14.0	0.5	13.5	14.5	Palma Sola massif (inclusive the Miocene calc-alkaline rocks)	EAP	4	4/5
14.7	0.3	14.3	15.0	Chiconquiaco–Palma Sola area	EAP	3	5
15.0	0.2	14.9	15.2	Mexico Basin	TMVB	1	
15.6	0.5	15.1	16.1	Chiconquiaco–Palma Sola area	EAP	3	
17.0	0.6	16.4	17.6	Palma Sola massif (inclusive the Miocene calc-alkaline rocks)	EAP	4	6/7
20.0	0.7	19.3	20.7	Tampico plain	EAP	4	8
21.0	0.6	20.4	21.6	Sierra de Tamaulipas	EAP	4	
21.6	0.3	21.3	21.9	Rio Grande de Santiago (Guadalajara)	TMVB	2	
21.6	0.3	21.3	21.9	Rio Grande de Santiago (Guadalajara)	TMVB	2	
23.2	0.3	22.9	23.5	Mexico Basin	TMVB	1	
23.5	0.7	22.8	24.2	Sierra de Tamaulipas	EAP	4	
28.0	0.8	27.2	28.8	Sierra de Tamaulipas	EAP	4	

Cholula-1EXP Events		
Event	Min Age (Ma)	Max Age (Ma)
Event 1	5.9	6.9
Event 2	8.3	8.3
Event 3	12.2	12.4
Event 4	12.2	13.5
Event 5	13.5	14.9
Event 6	16.4	16.4
Event 7	17.5	18.3
Event 8	18.3	19.3

Figure 15. Summarized geochronological data from different onshore Mexican volcanic centres believed to have been active during the age interval of interest compared with Cholula-1EXP. Eastern Alkaline Province (EAP), Los Tuxtlas Volcanic Field (LTVF), Trans MexicanVolcanic Belt (TMVB). Derived from publications 1: Arce et al, 2019; 2: Alva-Valdivia et al, 2000; 3: Ferrari et al, 2005; 4: Cantagrelet al, 1979 & 5: Nelson & Gonzalez-Caver, 1992. Cholula-1EXP event numbers correspond to those shown in Figure 5. Compare with figure 16.

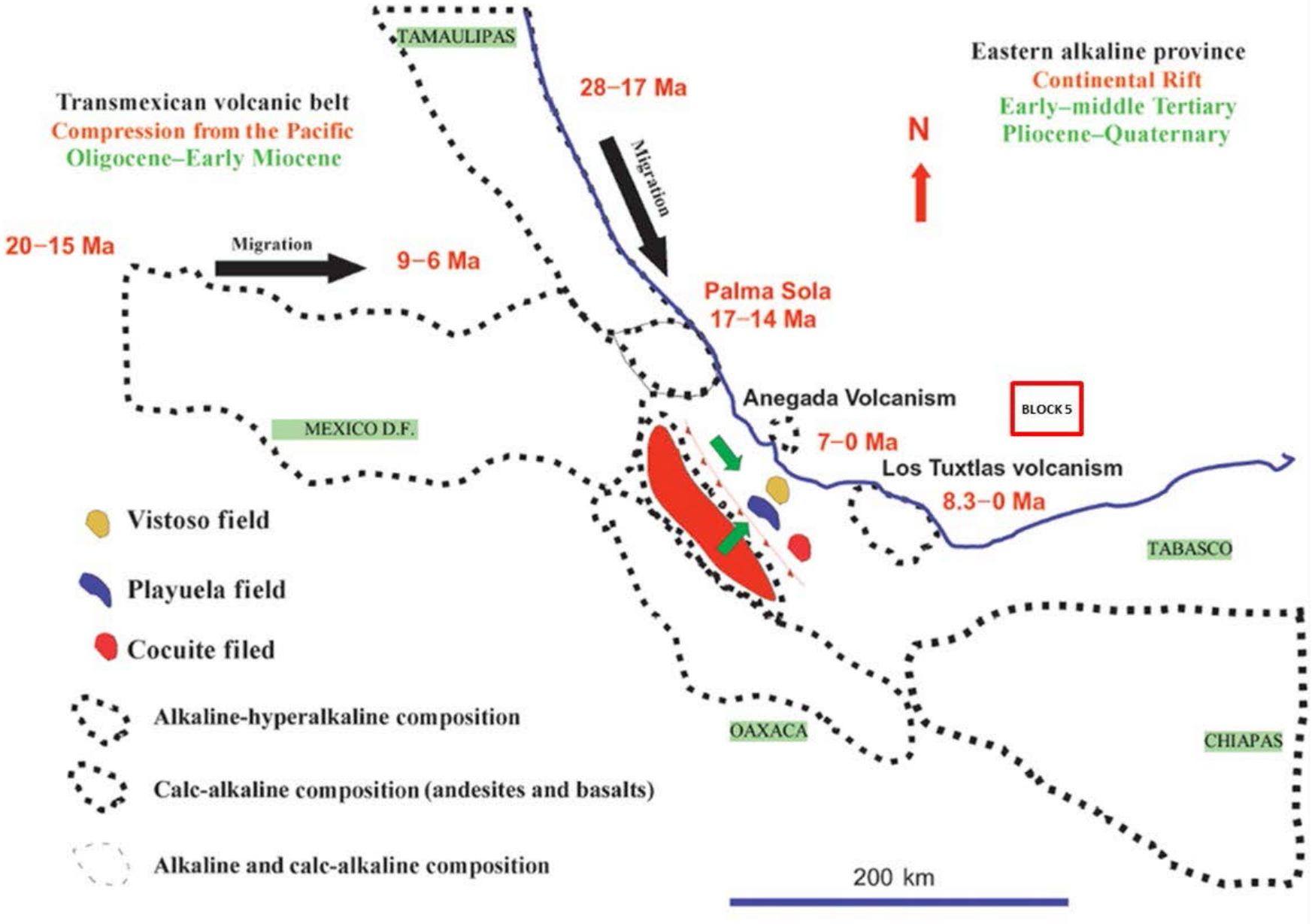

Figure 16. Onshore Mexican volcanic centres with respective ages of volcanic episodes and composition. Compare with figure 15. Modified from Gutiérrez Paredes et al, 2009.